The Influence of Charge Correlation and Ion Solvation on the Phase Behavior of Single-Ion Conducting Polymer Blend Electrolytes Using SAXS/SANS

Hsin-Ju Wu[1], Lilin He[2], William M. Breining[3], David M. Lynn[1,3], Whitney S. Loo[1,]*

[1]Department of Chemical and Biological Engineering, University of Wisconsin—Madison, 1415 Engineering Drive, Madison, Wisconsin 53706, United States

[2]Neutron Scattering Division, Oak Ridge National Laboratory, Oak Ridge, Tennessee 37831-6393, United States

[3]Department of Chemistry, University of Wisconsin—Madison, 1101 University Avenue, Madison, Wisconsin 53706, United States

[*]Corresponding Author email: wloo@wisc.edu

KEYWORDS: Polymer Blends, Electrolytes, Scattering

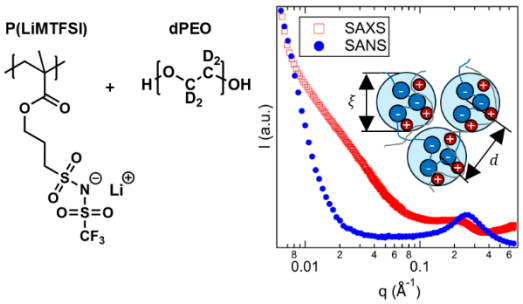

For Table of Contents use only

ABSTRACT

Single-ion conducting polymer blend electrolytes (SICPBs) have demonstrated exceptional electrochemical performance as solid-state battery electrolytes; however, their nanoscale morphology and thermodynamic behavior remain unexplored. In this work, we investigate blends composed of deuterated poly(ethylene oxide) and poly[lithium sulfonyl(trifluoromethane sulfonyl)imide methacrylate], dPEO/P(LiMTFSI), and report the first experimental study of the nanostructures of charge-neutral polymer blends using small-angle neutron scattering (SANS) and small-angle X-ray scattering (SAXS). Despite the macroscopic miscibility indicated by a single glass-transition temperature, SANS and SAXS results reveal disordered, charge-correlated nanostructures that are strongly influenced by blend composition and temperature. At low concentrations of charge polymer, the scattering is dominated by concentration fluctuations, and the random phase approximation is applied to extract values of the Flory-Huggins interaction parameter, χ_{SC}. At higher charged polymer content, concentration fluctuations are suppressed, and a correlation model is used to characterize the nanostructures of the charge correlations. We find that the structures of the charge correlations are highly dependent on blend composition—consistent with predictions from Sing's self-consistent field theory–liquid state models.

Understanding these features is essential for uncovering the ion transport mechanism that leads to improved electrochemical performance previously reported in SICPB systems.

INTRODUCTION

Polymer electrolytes have emerged as promising solid-state materials for energy storage due to their flexibility and safety advantages.[1] Poly(ethylene oxide) (PEO)/lithium bis(trifluoromethanesulfonyl) imide (LiTFSI) systems have been widely studied for solid-state battery applications due to their high ionic conductivity.[2,3] However, PEO-based electrolytes typically suffer from low cation transference numbers with recent reports demonstrating negative cation transference numbers at high salt concentrations ($r = [Li^+]/[EO] \geq 0.12$).[4,5] This phenomenon was attributed to the formation of concentrated ion clusters that ultimately hinder battery performance[6]. One strategy to improve the cation transference number is to eliminate ion concentration gradients by reducing the mobility of the negatively charged ions[7]. Single-ion conducting polymers (SICPs), wherein anions are immobilized via covalent bonds to the polymer backbone, mitigate the formation of concentration gradients and promote lithium-ion motion[8]. Nevertheless, SICPs often exhibit low ionic conductivities since the high glass-transition temperatures, T_g, typical of SICPs restrict segmental motion and further hinder ion transport.[8] To overcome the tradeoff between ionic conductivity and cation transference numbers, researchers have developed single-ion conducting polymer blends (SICPBs), which consist of an ion-containing polymer and an ion-conducting polymer. Previous studies on SICPBs have highlighted enhanced electrochemical performance including superionic transport[9] as well as improved electrochemical stability.[10] Although nanostructure is known to strongly influence ion

transport[11,12], these studies on SICPBs have assumed that miscible blends, identified by a single T_g, form a homogeneous phase rather than directly investigating their nanoscopic morphology.

The combination of small-angle neutron scattering (SANS) and small-angle X-ray scattering (SAXS) can provide complementary information on nanoscale morphology[13–16]. Specifically, neutrons provide good contrast between elemental isotopes, such as hydrogen and deuterium, making SANS particularly useful for studying hydrogen-containing materials like macromolecules. In contrast, X-rays are sensitive to electron density and are more suitable to distinguish between light and heavy elements. SANS results can be fitted to theoretical models in order to experimentally measure the Flory-Huggins interaction parameter, χ, between polymer chains and elucidate phase behavior at nanometer length scales.[13,14,17–21] Although no experimental SANS data currently exist for SICPB systems, several theories have been developed to describe the thermodynamics and nanostructures of polymer blends including salt-doped neutral homopolymer blends and polyelectrolyte blends[22–27]. One theory developed by Fredrickson and coworkers described the phase behavior of polyelectrolyte blends comprised of two oppositely charged polyelectrolytes[25,28]. Through the construction of a field-theoretic model that accounts for dielectric contrast and ion solvation effect, they showed that the competition between electrostatics and counterion entropy can lead to either macro- or microphase separation. The oppositely charged polyelectrolytes form electrostatically stabilized microphases with morphologies similar to those observed in block copolymers, e.g., lamellar, body center cubic, and hexagonally packed cylinder phases. Another theory developed by Sing and Olvera de la Cruz[22,29,30] incorporates charge correlation from liquid state theory (SCFT-LS) within the random phase approximation (PRA) framework previously developed by de Gennes[31,32] to derive a new expression for the structure factor of SICPBs, i.e., charge-neutral polymer blends. This expression extends RPA for uncharged

binary polymer blends by introducing correction terms, characterized by a new parameter, α, to account for electrostatics through an effective interaction parameter, $\chi_{eff} = \chi - \alpha$, which reflects the local charge structure.[30] The results of that past study show that χ_{eff}, and therefore α, is highly dependent on polymer blend properties, including blend composition, electrostatic interaction strength, and the charge density of the charged polymer component.

This study aimed to experimentally probe the phase behavior of SICPBs and compare our findings with previously developed theoretical models. We prepared blends of two polymers, deuterated PEO (dPEO) and poly[lithium sulfonyl(trifluoromethane sulfonyl)imide methacrylate] (PLiMTFSI), to investigate the effect of mixing ratio, *r*, temperature, and dPEO molecular weight on the nanostructure of SICPBs using SANS and SAXS. All blends prepared for this study were found to be macroscopically miscible, with each exhibiting a single T_g. The SANS profiles were dominated by contrast between the hydrogenated backbone of P(LiMTFSI) and the deuterated backbone of dPEO, highlighting interactions between polymer chains, while SAXS profiles primarily capture scattering from the fluorine-containing anions. By comparing results from both techniques with a theoretical model inspired by the work of Sing and coworkers[29,30], we find that the interplay between ion solvation and electrostatic interactions governs the nanostructure and phase behavior of the blends. For instance, blends with low ion concentrations exhibited lower critical solution temperature (LCST) behavior, while blends with higher ion concentrations displayed upper critical solution temperature (UCST) behavior. Through this study, we provide the first experimental dataset that investigates the nanostructures of charge-neutral polymer blends and demonstrate that the blend phase behavior is highly dependent on blend composition.

MATERIALS AND METHODS

Chemicals

Potassium 3-sulfopropyl methacrylate (98%, Sigma-Aldrich, USA), oxalyl chloride (98%, Sigma Sigma-Aldrich, USA), potassium bifluoride (KHF_2, 99%, Sigma-Aldrich, USA), trifluoromethanesulfonamide (95%, Sigma Sigma-Aldrich, USA), acetonitrile (ACN, ≥99.5%, Sigma-Aldrich, USA), dimethylformamide (DMF, anhydrous, 99.8%, Sigma-Aldrich, USA), dichloromethane (DCM, anhydrous, ≥99.8%, contains 40~150 ppm amylene as stabilizer, Sigma-Aldrich, USA), diethyl ether (Fisher Scientific, USA), 2-cyano-2-propyl benzodithioate (>97%, Sigma-Aldrich, USA), acetone (≥99.5%, Sigma-Aldrich, USA), dimethyl sulfoxide-d_6 (DMSO-d_6, 99.9 atom % D, contains 0.03% (v/v), Sigma-Aldrich, USA), sodium sulfate (Na_2SO_4, ≥99.0%, anhydrous, Sigma-Aldrich, USA), calcium carbonate ($CaCO_3$, ≥99.0%, Sigma-Aldrich, USA), butylated hydroxytoluene (BHT, ≥99%, Sigma-Aldrich, USA), potassium carbonate (K_2CO_3, ≥ 99.0%, Sigma-Aldrich, USA), calcium gluconate (monohydrate, DOT Scientific, USA), methanol (≥99.8%, Sigma-Aldrich, USA), and sodium chloride (NaCl, ≥99%, Sigma-Aldrich, USA) were used as received. Azobisisobutyronitrile (AIBN, Sigma-Aldrich, USA) was purified by recrystallization from methanol, involving dissolution at 50 °C followed by cooling in a freezer to induce crystal formation

Monomer Synthesis

The three-step synthesis of the potassium sulfonyl(trifluoromethane sulfonyl)imide methacrylate (KMTFSI) monomer was performed following the procedure reported by Lee[33] as outlined in **Scheme S1**. In the first step, 120 mL of anhydrous DCM was added to a dried 250 mL three-neck Schlenk flask under a nitrogen atmosphere. The solution was cooled to 0 °C, and a catalytic amount

of DMF (2 mL) was added dropwise, followed by the slow addition of oxalyl chloride (9.5 mL), during which gas release was observed After stirring for 30 min at room temperature, the mixture was cooled to 0 ℃ and 20 g of potassium 3-sulfopropyl methacrylate and 10 mg of BHT were added under a positive nitrogen atmosphere. The reaction proceeded overnight at room temperature in the dark, then quenched with water. The organic layer was extracted and washed thoroughly with deionized water five times, followed by two washes with saturated NaCl solution (brine). The organic layer was dried over anhydrous Na_2SO_4 until free-flowing crystals formed, then filtered and concentrated by rotary evaporation. The resulting transparent dark yellow oil of 3-propylsulfonylchloride methacrylate was obtained (18.27 g, 99.3% yield).

In the second step, 3-propylsulfonylchloride methacrylate was dissolved in 80 mL of ACN in a 250 mL Nalgene beaker Separately, 12.6 g of KHF_2 was dissolved in 35 mL of deionized water in a 250 mL of perfluoroalkoxy alkane (PFA) round-bottom flask. The ACN solution was added slowly to the KHF_2 solution using a polypropylene funnel and the reaction mixture was stirred at room temperature for 4 hrs. Afterward, the solution was poured into a 1 L Nalgene beaker and diluted with 200 mL of DCM. 140 mL of deionized water was added to promote phase separation. The organic and aqueous layers were separated using a separatory funnel. The aqueous layer was immediately diluted and neutralized with $CaCO_3$ in plastic containers. The DCM layer was washed thoroughly with deionized water five times, followed by two washes with brine. It was then dried over anhydrous Na_2SO_4, filtered, and concentrated by rotary evaporation to yield 3-propylsulfonylfluoride methacrylate as a clear, light-yellow oil (16.30 g, 96.2% yield).

Finally, 3-propylsulfonylfluoride methacrylate and 9.5 g of trifluoromethanesulfonamide were dissolved in 65 mL of ACN in a 100 mL three-neck glass flask. 29.0 g of K_2CO_3 was added, and the mixture was refluxed at 65 ℃ under nitrogen overnight. After completion, the mixture was

filtered to remove K_2CO_3 solids, and the filtrate was concentrated via rotary evaporation. The crude product was recrystallized by DCM to yield white KMTFSI powder (10.10 g, 86% yield). ^{1}H- and ^{19}F-NMR spectra were confirmed in DMSO-d_6 using a Bruker AVANCE III 400 NMR spectrometer as shown in **Figure S1** and **Figure S2**, respectively.

P(LiMTFSI) Synthesis

Poly[potassium sulfonyl(trifluoromethane sulfonyl)imide methacrylate], P(KMTFSI), was synthesized by reversible addition-fragmentation chain-transfer polymerization (RAFT) (**Scheme S2**). Briefly, KMTFSI, azobisisobutyronitrile, and 2-cyano-2-propyl benzodithioate were fully dissolved in DMF (8.5 mL) in a 25 mL Schlenk flask. After three freeze-pump-thaw cycles, the flask was filled with nitrogen and heated at 70 ℃ for 24 hr. The product was precipitated into diethyl ether and recovered using methanol three times. The polymer was dried at 60 ℃ under a high vacuum for 24 hr. Gel permeation chromatography (GPC) experiments were conducted using a Wyatt Dawn Heleos multi-angle light scattering (MALLS) and a Wyatt Optilab T-Rex refractive index (RI) detector. Two in-line columns were used: an Agilent PLgel 10 µm 10^3 Å column and an Agilent Resipore column. The molecular weight and polydispersity index, $Đ$, of P(KMTFSI) were measured using DMF as the mobile phase with a flow rate of 1 mL/min (**Figure S5)**. The GPC results of homopolymers are summarized in **Table S1**. ^{1}H- and ^{19}F-NMR spectra were recorded in dimethyl sulfoxide-d_6 using a Bruker AVANCE III 400 NMR spectrometer (**Figure S3** and **Figure S4**).

P(KMTFSI) and 4 equivalents of 0.2 M lithium chloride (99%, Sigma-Aldrich, USA) were stirred at room temperature overnight to facilitate ion exchange of potassium ions with lithium ions. The excess lithium chloride was removed by dialysis against deionized (DI) water (MWCO: 1 kDa)

for 3 days. The resulting light pink P(LiMTFSI) powder was obtained after freeze-drying for 4 days and subsequently stored in an argon glovebox (MBraun) with water and oxygen levels maintained at less than 1 ppm.

Preparation of Polymer Blends

The SICPB system investigated here consists of deuterated PEO (dPEO) and P(LiMTFSI), where dPEO was utilized to enhance neutron contrast and facilitate structural characterization. A series of PEO/P(LiMTFSI) blends with varying mixing ratios and polymer molecular weights were prepared in a glovebox, with their compositions summarized in **Table S2**. The dPEO was purchased from Polymer Source (Dorval, Quebec, Canada) and dried under vacuum in the antechamber of a glovebox for 24 h and then transferred into the glovebox. P(LiMTFSI) and dPEO were dissolved in anhydrous methanol separately to a concentration of 10 mg/mL and stirred overnight. A variety of dPEO/P(LiMTFSI) blends with different values of mixing ratio $r = [P(LiMTFSI)]/[dPEO]$ and prepared using polymers of varying molecular weight were prepared in the glovebox. The solutions were blended and stirred at 70 ℃ for a minimum of 12 h. Once the solutions were fully mixed, the caps were removed from the vials and the solvent was allowed to evaporate. After drying on a hotplate at 70 °C overnight, the polymer blends were transferred into a vacuum oven and dried under vacuum for 72 h at 90 °C to remove the residual solvent.

Differential Scanning Calorimetry (DSC) Analysis

Polymer samples ranging from 2 to 10 mg were hermetically sealed in aluminum pans in a glovebox. DSC experiments were performed using a TA Instruments Q100 instrument using two heating and cooling cycles. The heating rate was 10 ℃/min and the cooling rate was 5 °C/min over

a temperature range of -80 ℃ to 200 °C. The melting temperature (T_m) and T_g were determined from the second heating cycle.

Small-Angle Neutron Scattering (SANS) Measurements

The dPEO/P(LiMTFSI) blends were prepared by melting into a copper 3.5 cm × 4.5 cm × 2.2 cm sample holder in a glovebox and then sandwiched between two 2.54 cm outer diameter quartz windows with 1.66 mm spacing. The assembled samples were degassed in the glovebox antechamber at 110 ℃ for 30 minutes. Temperature-dependent SANS experiments were conducted on the GP-SANS (CG-2) beamline at Oak Ridge National Lab (ORNL), Neutron Science Directorate[34]. The SANS experiments were performed at 70, 90, 110, and 130 °C with a q range of 0.005 to 0.5 $Å^{-1}$. The SANS intensity, $I(q)$, was recorded as a function of the magnitude of the scattering wavevector, defined as $q = \frac{4\pi}{\lambda}\sin(\frac{\theta}{2})$, where θ is the scattering angle and λ is the wavelength of the neutron beam. Background scattering from the instrument and sample holder was subtracted during data reduction and standard corrections were applied for detector efficiency, sample thickness, and transmission. The final scattering intensity was placed on an absolute scale using a pre-calibrated standard.[35]

Small-Angle X-ray Scattering (SAXS) Measurements

The dPEO/P(LiMTFSI) blends were prepared by melting the polymer blends at 90 ℃ into a stainless-steel holder with a 4 mm inner diameter and a 0.554 mm wall thickness. The samples were annealed at 90 °C in a vacuum oven for at least 24 h to remove bubbles. After this, the heater was turned off and the samples were slowly cooled under vacuum. Kapton polyimide tape was used to seal the prepared samples. Temperature-dependent SAXS measurements were performed using a Xeuss 3.0 system. Measurements were performed every 20 °C from 50 °C to 130 °C with

an exposure time of 900 seconds in high-intensity mode. Samples were allowed to equilibrate at each temperature for 20 minutes prior to measurement. The resulting 2D scattering patterns were isotropic and were azimuthally integrated into 1D profiles using XSACT Pro advanced data analysis software. Background intensities from the Kapton tape were subtracted from the total intensity. The SAXS intensity, $I(q)$, was recorded as a function of the magnitude of the scattering wavevector, defined as $q = \frac{4\pi}{\lambda}\sin(\frac{\theta}{2})$, where θ is the scattering angle and λ is the X-ray wavelength.

RESULTS AND DISCUSSION

Blend Preparation and Characterization

The SICPB system investigated here consists of deuterated PEO (dPEO) and poly[lithium 3-(methylacryloxy)propylsulfonyl-1-(trifluoromethanesulfonylimide)] (P(LiMTFSI)); the structures of these polymers are shown in **Figure 1**. The poly(methyl methacrylate) (PMMA)-based single-ion conducting polymer was chosen to increase miscibility as blends of PEO and PMMA are known to have negative values of χ.[18,36] The molecular weights and polydispersity indices of homopolymers are listed in **Table S1**, while the polymer blends were prepared as detailed in **Table S2**. Sample names are defined as "$M_{n,dPEO}/M_{n,P(LiMTFSI)}/r$", where r is the mixing ratio is calculated as the molar ratio of lithium ions to deuterated ethylene oxide monomers, given by $r = [Li^+]/[dEO] = [P(LiMTFSI)]/[dPEO]$.

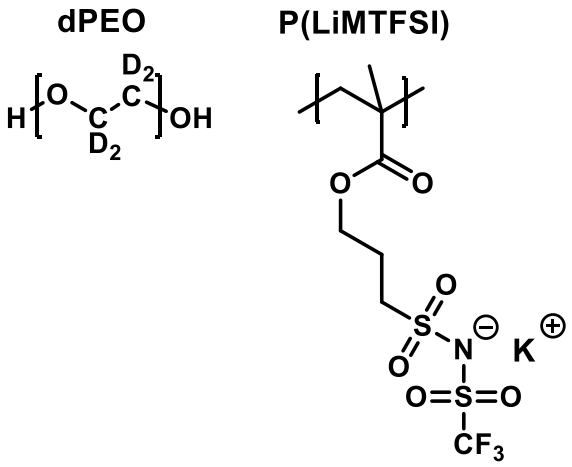

Figure 1. Chemical structures of the deuterated poly(ethylene oxide) (dPEO) and poly[lithium sulfonyl(trifluoromethane sulfonyl)imide methacrylate] (P(LiMTFSI)) SICPB system used in this study.

Differential scanning calorimetry (DSC) was used to measure the thermal properties of polymer blends and screen for miscibility. **Figure 2(a)** shows the DSC results for blends of 30 kDa dPEO and P(LiMTFSI). The T_g of pure P(LiMTFSI) was measured to be 112.4 °C, while the T_g of dPEO was measured to be -48.5 °C. Neat dPEO is semi-crystalline with a T_m of 62.5 °C. All blends exhibited a single $T_{g,blend}$ between two homopolymers, which can be attributed to the attractive ion-dipole interactions between P(LiMTFSI) and dPEO[9]. The $T_{g,blend}$ increases with increasing values of r, i.e., increasing concentration of P(LiMTFSI), consistent with the findings of Olmedo-Martínez *et al.*[37], with the presence of a single $T_{g,blend}$ being widely accepted as evidence for macroscopic miscibility, indicating that the system is not macrophase separated, i.e., forms a single-phase[38,39]. Similar to PEO/LiTFSI blends[40], the crystallinity of dPEO is suppressed with increasing P(LiMTFSI) content. For $r > 0.10$, no T_m was observed, indicating that the blends are fully amorphous. A sharp T_m peak was observed when r = 0.05, suggesting a coexistence of

dPEO-rich semi-crystalline domains and an amorphous phase entangled with P(LiMTFSI) below T_m. DSC results for 10 kDa dPEO/P(LiMTFSI) blends shown in **Figure S6(a)** followed similar trends. The weak melting peak for r = 0.10 indicates minimal crystallinity, consistent with the behavior observed in the 30 kDa blends.

The effect of blend composition, quantified by the weight fraction of the P(LiMTFSI), w_{Li}, on the thermal transitions described by $T_{g,blend}$ is shown in **Figure 2(b).** The black squares represent $T_{g,blend}$ values taken from DSC thermograms in **Figure 2(a)**. The Gordon-Taylor equation has been used previously to describe $T_{g,blend}$ in ion-containing polymer blends, as it accounts for non-ideal mixing behavior through a fitted parameter, k, which reflects interactions between the polymer components[9,10]. The solid line in **Figure 2(b)** represents the fit using the Gordon-Taylor equation according to **Eq (1)**:

$$T_{g,blend} = \frac{w_1 T_{g,1} + k w_2 T_{g,2}}{w_1 + k w_2} \quad (1)$$

where w_1 and w_2 are the weight fractions of dPEO and P(LiMTFSI), $T_{g,1}$ and $T_{g,2}$ are the T_g values of dPEO and P(LiMTFSI), and k is an adjustable parameter. We excluded the $T_{g,blend}$ value at r = 0.05 from the fit in **Figure 2(b)**, as it is well known that the presence of semi-crystalline domains can affect the observed value for T_g.[41] The fitted parameter, k, quantifies the strength of intermolecular interactions between the polymer components[42]. For 30 kDa dPEO/P(LiMTFSI) blends, the value of k was determined to be 0.44 $\pm$ 0.04, indicating intermediate ion-dipole interactions between dPEO and PLiMTFSI. This value matches previous results reported for similar ion-containing polymer blends.[10,43]Additional thermal data for blends prepared with 10 kDa dPEO are shown in **Figure S6(b)**. Decreasing the molecular weight of dPEO

from 30 kDa to 10 kDa shifts the values of $T_{g,blend}$ to lower temperatures by approximately 1~2 °C for each blend composition because of the difference in the $T_{g,dPEO}$ values with different $M_{n.dPEO}$. The fitted k value for 10 kDa dPEO/P(LiMTFSI) blends was 0.50 ± 0.04, which is quantitatively similar to the value for the 30 kDa dPEO/PLiMTFSI blends, indicating that the intermolecular interactions are not significantly affected by dPEO molecular weight. Previous work has demonstrated that the molecular weight of P(LiMTFSI) significantly influences thermal properties of similar blends[10]. Therefore, our results suggest that the intermolecular interactions responsible for non-ideal mixing originate primarily from the P(LiMTFSI) moieties. While tuning the dPEO properties can alter the segmental dynamics of the blend, as indicated by changes in $T_{g,blend}$, it does not substantially change the degree of non-ideal mixing in SICPBs because dPEO acts primarily as a solvent in these systems.

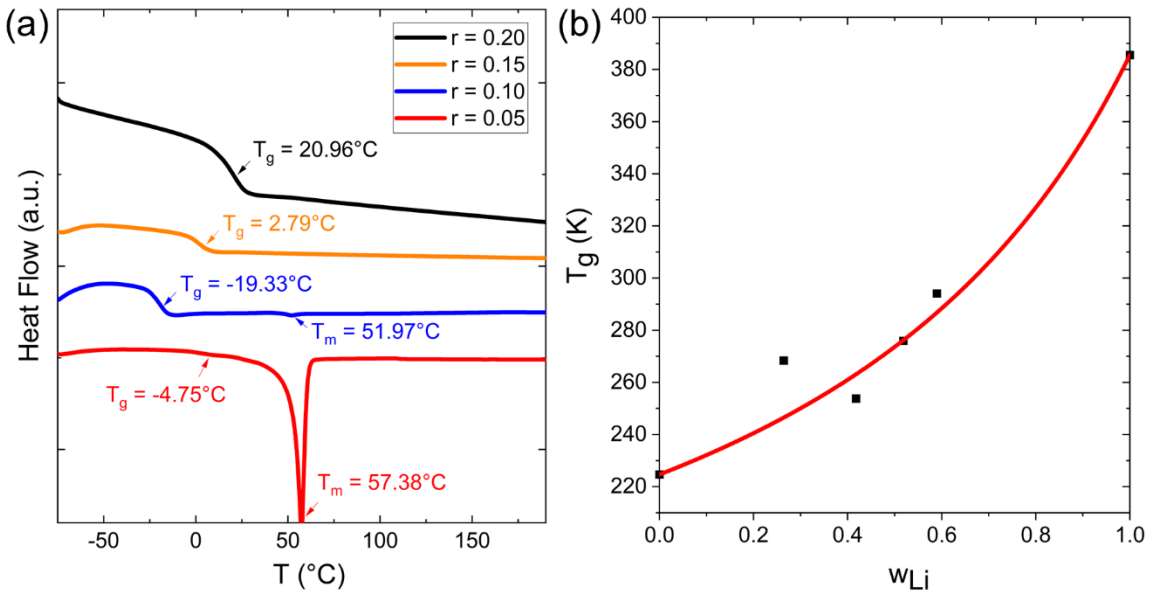

Figure 2. (a) Differential scanning calorimetry (DSC) traces of 30 kDa dPEO/P(LiMTFSI) blends at various values of r. (b) The $T_{g,blend}$ of 30 kDa dPEO/P(LiMTFSI) as a function of

weight fraction of P(LiMTFSI), w_{Li}. The red solid line represents the fit using the Gordon-Taylor equation.

Resolving nanoscopic structure with SANS and SAXS

As part of this study, we aimed to provide experimental datasets that could be used to investigate the nanostructures of charged–neutral polymer blends (i.e., SICPBs) using both SANS and SAXS. The thermodynamic behavior of SICPBs is governed by a combination of polymer backbone interactions, ion solvation, and electrostatic interactions. The SANS scattering contrast arises primarily from differences between the deuterated PEO backbone and the hydrogenated P(LiMTFSI) backbone and, therefore, enables the determination of: (1) the miscibility of the polymer blends, (2) the presence of charge correlations, and (3) the experimental value of the Flory–Huggins interaction parameter taken from scattering, χ_{sc}. **Figure 3(a)** shows the SANS profiles of 30 kDa dPEO/P(LiMTFSI) blends at 90 °C for various values of r. Inspection of these profiles reveals the qualitative features of these SANS profiles to depend strongly on r. For example, the scattering contribution from the polymer chains dominates at r = 0.05 (red trace), reflecting disordered concentration fluctuations[20]. While the observation of a single T_g, as discussed above, suggests that the blends are macroscopically miscible, the SANS profiles indicate a nanoscale disordered structure similar to what is observed in block copolymers at low values of segregation strength, χN. We hypothesize that this disordered structure arises from nanoscale phase separation between the semi-crystalline and amorphous domains, as suggested by the DSC traces (**Figure 2a**). Previous experimental studies have also observed nanoscale phase separation between the semi-crystalline PEO domains in optical micrographs in different SICPBE systems at high PEO concentrations.[44] As r increases to 0.10 (blue trace) and more P(LiMTFSI) is introduced

to the system, electrostatic interactions become more prominent and a correlation peak emerges in the high-q region. The disappearance of the mid-q feature in the SANS profile suggests that concentration fluctuations are suppressed due to strong ion-dipole interactions. Similar effects have been observed in lithiated single-ion conducting block copolymers[45] and polyamide/ionomer blends[14], where ion dissociation and strong intermolecular interactions enhance miscibility. With further increasing in P(LiMTFSI) concentration, i.e., increasing r (orange and black traces), the high-q correlation peak broadens and shifts to higher q-values. These changes suggest that the average distance between charge correlations decreases and the correlations become more polydisperse. Theoretical predictions by Sing and coworkers using a hybrid of self-consistent field theory–liquid-state theories (SCFT-LS) also found that strong local ion correlations at low polyelectrolyte content (analogous to low r in our system) in charge-neutral polymer blends can lead to phase separation.[22,29,30] Across all blend compositions, the low-q region of the SANS profiles consistently exhibits a q^{-4} power-law behavior, which was previously observed for other ion-containing polymers and was attributed to voids[13,46] resulting from insufficient degassing and may not reflect intrinsic structural features of the blends[18,47,48]. Additional SANS data for blends prepared with 10 kDa dPEO are provided in **Figure S8(a)** and show qualitatively similar results.

Figure 3(b) shows the SAXS profile of 30 kDa dPEO/P(LiMTFSI) blends at various values of r at 90°C. The SAXS contrast depends on the electron density differences within the system, and thus, provides information regarding the distribution of the tethered anions in the melt phase. At r = 0.05 (red trace), an obvious shoulder appears at around q = 0.2 Å^{-1}, reflecting the presence of ionic domains with an average interdomain spacing of ~3.1 nm. Similar features have been reported in SAXS profiles for single-ion conducting block copolymers, with an ionomer peak around q = 0.25 Å^{-1}.[45] Therefore, the SAXS data reported here are consistent with our DSC and

SANS results, suggesting that the formation of semi-crystalline domains in the SICPBs can drive nanoscale phase separation. Our results also suggest that when the blend is heated above T_m, the ordered crystalline structure breaks down and attractive ion-dipole interactions between dPEO and lithium-ions promote mixing between the two polymers. As a result, the combination of disordered dPEO/P(LiMTFSI) entanglements and charge correlations gives rise to nanostructures that are polydisperse in size and shape and heterogeneously distributed throughout the blend. This interpretation is consistent with the broad shoulder observed by SAXS and the disordered concentration fluctuations observed by SANS.

As charge concentration increases to r = 0.10 (blue trace) in **Figure 3(b)**, the shoulder in mid-q region becomes weaker and the low-q slope becomes steeper, suggesting a reduction in concentration fluctuations. At $r \geq 0.15$ (orange and black traces), the SAXS profile becomes featureless without an evident shoulder, implying that the blends become more homogeneously disordered at higher charge concentrations. This apparent increase in miscibility is likely due to the preferential solvation of lithium-ions by the dPEO chains over the P(LiMTFSI) chains, which has been previously observed in single-ion conducting block copolymers[49,50]. Segalman and coworkers also observed similar behavior in dry ionic blends of conjugated polyelectrolytes and polymeric ionic liquids[28], where increased charge density stabilized the blends and increased miscibility. Based on the SANS and SAXS data, we believe that all SICPB compositions studied form disordered phases that are macroscopically miscible yet exhibit nanoscale heterogeneity. This suggests that our blends lie below the order-disorder transition on the phase diagram, i.e., at low χN [25]. Similar trends are observed for 10 kDa dPEO blends, as shown in **Figure S8(b)**. We find that both charge correlations and ion-dipole interactions likely play vital roles in governing the thermodynamics and resulting nanoscale morphology of the SICPBs.[23]

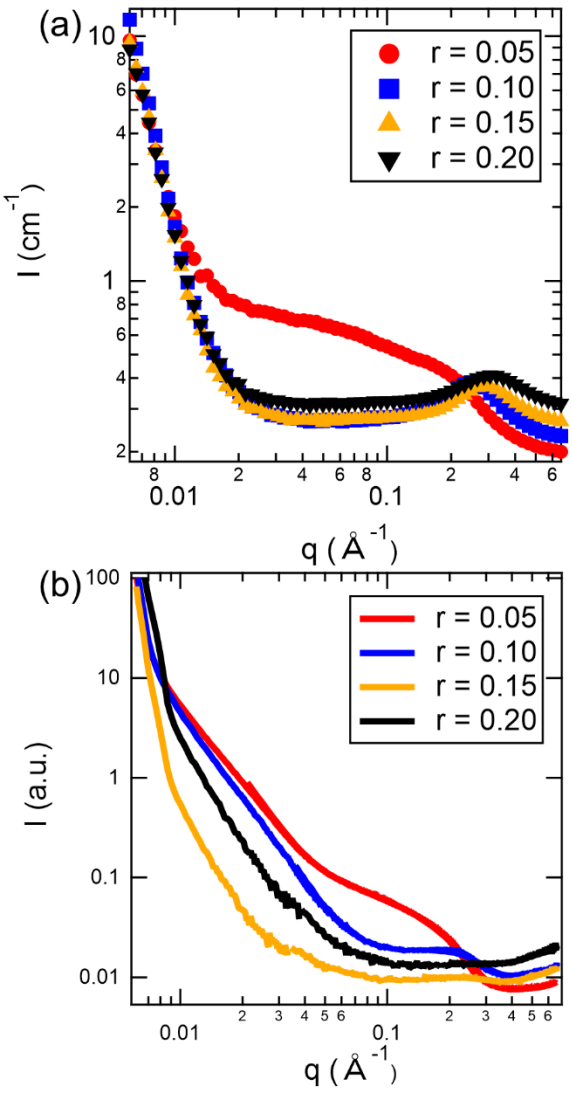

Figure 3. (a) Small-angle neutron scattering (SANS) and (b) small-angle X-ray scattering (SAXS) profiles for 30 kDa dPEO/P(LiMTFSI) blends at various mixing ratios, r, at 90°C. Error bars in (a) represent the standard deviation and are smaller than the data points.

To quantitatively extract structural insights from our SANS data, we developed a composite model inspired by Sing's theory for charge-neutral polymer blends[30] as shown by **Eq (2)**. This composite model includes: (1) a power-law term for low-q region, (2) random phase approximation (RPA)

for an uncharged system in the mid-q region, and (3) a Lorentzian peak model for high-q features induced by charge correlations.

$$I_{total}(q) = I_{power}(q) + I_{RPA}(q) + I_{Lorentzian}(q) + I_{incoherent} \quad (2)$$

The contribution from the incoherent scattering, $I_{incoherent}$, was determined using previous methods[13]. The de Gennes's RPA theory accounts for the mid-q scattering and is commonly used to describe miscible binary polymer blends. It allows for extraction of χ_{sc} from scattering data as shown in **Eq (3)**:[18,51,52]

$$I_{RPA}(q) = v_{ref}(B_{dPEO} - B_{PLiMTFSI})^2 \left[\frac{1}{S_{11}} + \frac{1}{S_{22}} - 2\chi_{sc}\right]^{-1} \quad (3)$$

where v_{ref} is the reference volume (taken here to be 0.1 nm^3),[17–19] B_i is the scattering length density of the species i, S_{ii} is the ideal structure factor of species i,[13] and χ_{sc} is the Flory-Huggins interaction parameter, which quantifies the strength of repulsion between different polymer chains. B_i is given by **Eq (4)**:

$$B_i = \frac{b_i}{v_i} \quad (4)$$

where b_i is the neutron scattering length and v_i is the molar monomer volume of species i. The neutron scattering lengths for dPEO and P(LiMTFSI) are 4.58×10^{-12} cm and 7.70×10^{-12} cm, respectively. The molar monomer volume for dPEO was taken from the literature as 41.34 cm^3/mol[18] and the molar volume of P(LiMTFSI) was calculated using the group contribution approach from van Krevelen *et al.* to be 211.8 cm^3/mol[49,53]. The ideal structure factors, S_{ii}, are given by **Eq (5)**:

$$S_{ii} = \varphi_i N_i P_i(q) \tag{5}$$

where φ_i is the volume fraction of species i, N_i is the degree of polymerization of species i, and $P_i(q)$ is the form factor of species i. In this study, we choose to use a form factor for a Gaussian coil as given by **Eq (6)**:

$$P_i(q) = \left[\frac{\exp\left(-q^2 {R_{g,i}}^2\right) - 1 + q^2 {R_{g,i}}^2}{\left(q^2 {R_{g,i}}^2\right)^2}\right] \tag{6}$$

where $R_{g,i}$ is the radius of gyration of species i according to **Eq (7)**:

$${R_{g,i}}^2 = \frac{\alpha_i N_i {l_i}^2}{6} \tag{7}$$

where α_i is a chain stretching parameter that is used as a fitting parameter and l_i is statistical segment length of species i. The value of l_{dPEO} is 7.2 Å and the value of $l_{\mathrm{P(LiMTFSI)}}$ is approximated by the value for PMMA, which is 5.8 Å[18].

The correlation model, which includes the power law and Lorentzian peak terms ($I_{Correlation}(q) = I_{power}(q) + I_{Lorentzian}(q)$, from **Eq (2)** is introduced to describe the high-q scattering that characterizes the nanoscale structure of the SICPBs that arise due to the contributions from the charge correlations[54,55]:

$$I_{Correlation}(q) = \frac{A}{q^n} + \frac{C}{1 + (|q - q_0|\xi)^m} \tag{8}$$

where A is the Porod scaling factor, n is the Porod exponent, C is the Lorentzian scaling factor, q_0 is the position of the Lorentzian peak, ξ is the correlation length, and m is the Lorentzian exponent. The first Porod term accounts for the scattering from large-scale clustering, while the second

Lorentzian function describes features arising from Coulombic interactions between charged polymer segments.[24] Disordered concentration fluctuations are present in the r = 0.05 and 0.10 blends as evident by the mid-q broad shoulders in the SAXS data shown in **Figure 3(b).** Accordingly, we fit the SANS data to RPA model, I_{RPA}, **Eq (3)**, to extract the thermodynamic contributions from polymer backbones, quantified by χ_{SC}.

Figure 4(a) and **(b)** show the SANS profiles of 30 kDa dPEO/P(LiMTFSI) at r = 0.05 and 0.10, respectively, across a temperature range of 70 ℃ to 130 ℃, where the symbols represent the SANS data and the solid line shows the fit to **Eq (2)**. For the r = 0.05 blend in **Figure 4(a)**, the SANS intensity steadily increases with temperature indicating a strong temperature-dependence on the nanoscale structure[16,20]. Similar changes are observed in the same q-region of the SAXS profiles for r = 0.05 as shown in **Figure S9(a)**. As r increases to 0.10 and ion concentration increases (**Figure 4(b)**), the intensity contribution from I_{RPA} diminishes in the mid-q region, and instead, the scattering is dominated by the high-q Lorentzian peak captured by $I_{Lorentzian}$. Compared to the r = 0.05 blend (**Figure 4(a)**), temperature-dependent changes in SANS intensity are less pronounced for the r = 0.10 blend. For both r = 0.05 and 0.10 blends, the correlation peaks shift slightly toward lower q and broaden as the temperature increases from 70 ℃ to 130 ℃, indicating a temperature-induced change in domain spacing and correlation length. **Figure 4(c)** summarizes the extracted χ_{sc} values obtained from fitting **Eq (3)** as a function of inversion temperature. Empirically, the Flory-Huggins interaction parameter, χ, is often found to vary inversely with temperature, T:

$$\chi = A' + \frac{B'}{T} \tag{9}$$

where A' and B' are fitting parameters. The solid lines in **Figure 4(c)** show fits to **Eq (9)**. The value of B' is negative for the r = 0.05 blend, indicating that the blend exhibits lower critical solution temperature (LCST)-like behavior. This is consistent with the increasing SANS intensities observed in **Figure 4(a)** as temperature increases[20,56]. Previous studies of lithiated single-ion conducting block copolymers also reported LCST behavior[45]. At low r, corresponding to low ion concentrations, ion-dipole interactions weaken at higher temperatures, reducing miscibility and increasing χ_{SC}. As the P(LiMTFSI) concentration increases to r =0.10, the blend exhibits upper critical solution temperature (UCST)-like behavior, with the value of B' in **Eq (9)** becoming positive. The results in **Figure 4(c)** also show that, at most temperatures, the blends exhibit negative values of χ_{SC}, consistent with favorable interactions between dPEO and P(LiMTFSI). Only at 70 °C for the r = 0.10 electrolyte does χ_{SC} become positive, however even under these conditions it remains below the critical value for macrophase separation, e.g., $\chi_{crit} = \frac{1}{2}\left(\frac{1}{\sqrt{N_1}}+\frac{1}{\sqrt{N_2}}\right)^2 = 0.0134$.[57] The low values of χ_{SC} also correspond to low values of χN, further supporting our claim that our SICPB system lies in the disordered regime.

The results shown in **Figure 4(c)** agree quantitatively with the theoretical predictions for the effective interaction parameter, χ_{eff}, of charge-neutral polymer blends of Sing and coworkers[22,30], showing that the value of χ_{SC} and its temperature dependence vary with blend composition, r. In addition, their theory predicted phase separation at low volume fraction of charged polymers[29]. Our findings support these conclusions, as the blend with the lowest composition of P(LiMTFSI), r = 0.05, is located nearest to the order-disorder transition boundary. **Figure 3(a)** shows a distinct change in slope at $q \geq 0.3$ Å^{-1} for blend with $r \geq 0.15$, deviating from typical scaling of q^{-2} found in RPA. In addition, the SAXS profiles in **Figure 3(b)** do not exhibit the broad shoulders

associated with concentration fluctuations at $r \geq 0.15$. Attempts to fit the SANS profiles for $r = 0.15$ and 0.20 using the RPA model in **Eq (3)** did not yield reasonable values for χ_{SC}, consistent with the featureless SAXS data. Therefore, contributions from I_{RPA} were excluded from the fitting. All fitted parameters and associated errors from the fits to **Eq (2)** are provided in **Tables S3** and **S4** for 10 kDa dPEO/PLiMTFSI and 30 kDa dPEO/PLiMTFSI blends, respectively. **Figure S12** shows Kratky plots, where $\frac{q^2 S(q)}{\nu}$ is plotted against q, for the $r = 0.05$ blend at various temperatures to investigate the compactness of macromolecules and to calculate the statistical segment length of polymer chains[13,19,47]. This plot shows that the SICPB system does not exhibit a plateau at the high-q region, reflecting a slightly swollen behavior of the SIPBE due to the electrostatic interaction between the charged side chains on P(LiMTFSI). Similar features have been reported in charged polymer systems such as polyelectrolyte complexes[58] and ionomer solutions[59] due to the formation of ionic aggregates.

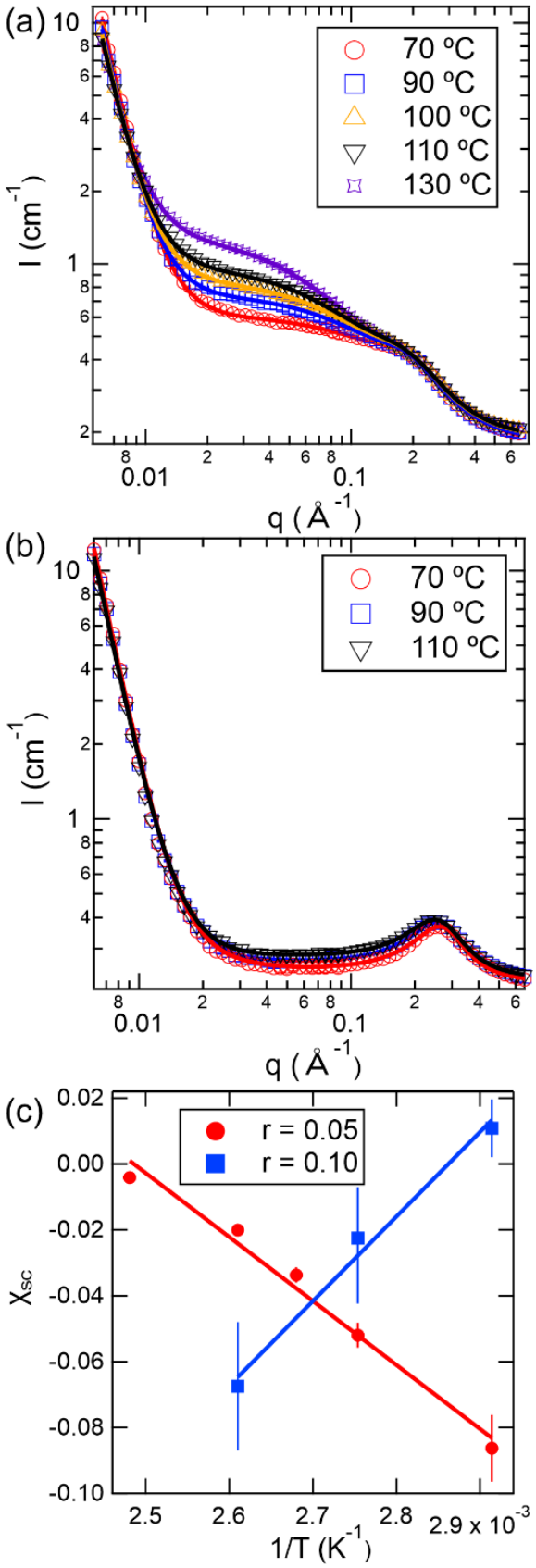
(a)
70 ºC
90 ºC
100 ºC
110 ºC
130 ºC
I (cm-1)
q (Å-1)
(b)
70 ºC
90 ºC
110 ºC
I (cm-1)
q (Å-1)
(c)
r = 0.05
r = 0.10
χsc
1/T (K-1)
2.9 x 10-3

Figure 4. SANS profiles and corresponding fits for 30 kDa dPEO/P(LiMTFSI) blends at various temperatures with mixing ratios of $r =$ (a) 0.05 and (b) 0.10. The solid lines represent fits to **Eq (2)**. (c) Temperature dependence of χ_{sc} determined from fitting the SANS data with **Eq (3)** for r = 0.05 (red) and r = 0.10 (blue). Error bars represent the standard deviation of the fitted value of χ_{SC}. Solid lines represent linear fits to the experimental data according to **Eq (9)**.

Figure 5 shows the results from fitting the correlation model, $I_{correlation}$ (**Eq (8)**), to the SANS profiles as a function of temperature, T, at a variety of mixing ratios, r. From these fits, two characteristic length scales describing the nanoscale morphology of the charged-neutral blends are extracted, as shown in **Figure 5(a)**. The interdomain spacing, $d = \frac{2\pi}{q_0}$, reflects the average distance between charge-correlated domains, while the correlation length, ξ, describes the characteristic size of local charge-correlated regions. **Figure 5(b)** plots d as a function of temperature for various values of r, with solid lines representing linear fits to the data. The value of d increases with increasing temperature for all r, implying that the structural changes arise from thermal effects rather than temperature-induced phase transitions. The temperature dependence of d is slightly stronger for the r = 0.05 sample (red trace), which matches the strong temperature dependence of the SANS data shown in **Figure 4(a)**. At a given temperature, d decreases as r increases, but the magnitude of this change diminishes at higher r. For instance, at 70 °C, the interdomain spacing for r = 0.05 (red trace) is 34.9 Å, which decreases significantly to 24.0 Å at r = 0.10 (blue trace). Further increasing the P(LiMTFSI) content to r = 0.15 (orange trace) results in a smaller decrease to 20.4 Å and the spacing remains relatively constant at 18.9 Å for r = 0.20 (black trace). This trend indicates that interdomain spacing is highly sensitive to the fraction of charged polymer at low P(LiMTFSI) concentrations but becomes relatively constant at higher concentrations. A

similar trend has been reported in PEO-based sulfonate ionomers[60], where the average interaggregate spacing also decreases as ion concentration increases, suggesting that the ionic aggregates are strongly influenced by the concentration of charged species.

Figure 5(c) plots ξ as a function of temperature for various values of r considered, where solid lines illustrate the linear relationship between ξ and temperature. For $r \leq 0.10$, ξ decreases with increasing temperature, indicating that the size of the charge correlations decreases as temperature increases. This temperature effect is more pronounced for the $r = 0.05$ sample (red trace) than for $r = 0.10$ (blue trace), similar to the trends observed for d. In contrast, for $r \geq 0.15$, ξ increases with increasing temperature, indicating that charge-correlated nanostructures grow in size at elevated temperatures. In other words, as temperature increases, the size of the charge-correlated nanostructures decreases and the distance between them increases for blends with $r \leq 0.10$. For blends with $r \geq 0.15$, both the size and spacing of charge correlations increase with temperature. Similar trends in r and T on d and ξ are observed in 10 kDa dPEO/P(LiMTFSI) blends shown in **Figure S10**. Compared with **Figure 5**, lower $M_{n,dPEO}$ does not significantly affect d and ξ, showing that $M_{n,dPEO}$ is not the primary factor influencing the thermodynamics and nanostructure of SICPBs. This finding is consistent with our DSC results, in which the fitted parameter k, quantifying non-ideal mixing, does not change significantly between blends prepared with 10 kDa and 30 kDa dPEO. Therefore, r appears to have the strongest influence on blend thermodynamics.

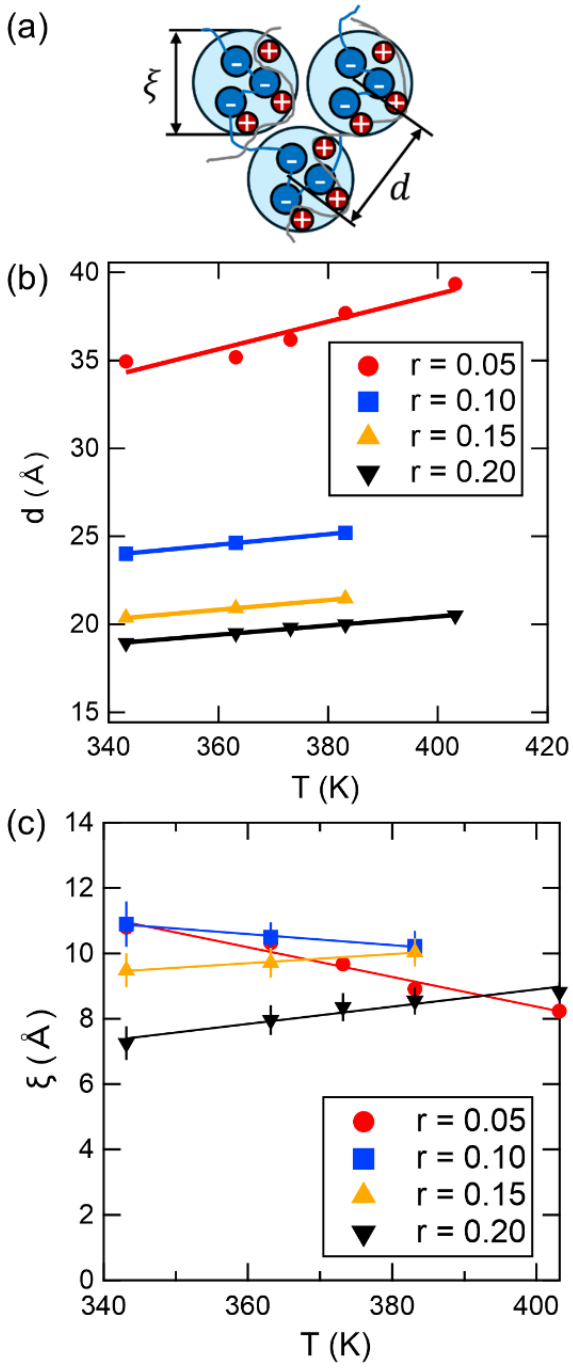

Figure 5. (a) Schematic illustration of charge-correlated region highlighting the interdomain spacing, d, and the correlation length, ξ. (b) The interdomain spacing and (c) the correlation length as a function of temperature, T, at various mixing ratios, r, of 30 kDa dPEO/P(LiMTFSI).

Solid lines represent linear fits to the experimental data. Error bars represent the standard deviation obtained from the fit to **Eq (8)**.

This study provides the first experimental dataset on the nanostructure of charge-neutral polymer blends and provides a useful basis for comparisons with previously developed theories. The model used to fit the SANS data includes two main contributions: the first is χ_{SC}, which quantifies the thermodynamics between the polymer backbones; the second includes the structural parameters, d and ξ, which describe the nanoscale features induced by charge correlations. According to the theory developed by Sing and coworkers[30], $\chi_{eff} = \chi - \alpha$, where α is a correction term that reflects local charge structure and is dependent on blend composition. We propose that d and ξ are directly related to α, and that our analysis effectively captures changes in χ_{eff} as a function of blend composition. For example, in the blend composition window where χ_{SC} was determined (r = 0.05 and 0.10), we observe significant differences in d and ξ, consistent with theoretical predictions that composition strongly influences thermodynamics and nanostructure. Unfortunately, the design of our SICPB system does not allow for independent tuning of the charge density and electrostatic interaction strength, both of which are critical parameters for understanding α and χ_{eff}. Thus, we cannot precisely determine which blend properties in our charge-neutral blends drive the observed structural changes. In addition, we choose to limit our discussion to temperature-related structural changes, as temperature influences many blend properties including χ_{SC}, dielectric constants[60], and electrostatic strengths. One parameter commonly used to quantify electrostatic strength is the Bjerrum length, which depends on both the dielectric constant and the temperature of the system[61]. Because these factors are inherently coupled, our experimental results do not allow us to distinguish their individual contributions to the observed structural changes. Future research will focus on designing tunable charged-neutral

polymer blend systems in which the strength of charge correlations and the charge density can be precisely controlled to further investigate blend thermodynamics.

CONCLUSIONS

We have reported the first experimental investigation of the nanostructure and phase behavior of a series of single-ion conducting polymer blends (SICPBs), dPEO/P(LiMTFSI), using SANS and SAXS. Although all blends investigated here were macroscopically miscible, as indicated by the observation of a single T_g, the structural analysis revealed nanoscale inhomogeneity arising from the interplay between charge correlations and ion-dipole interactions. At low content of charge polymer, the crystallinity of dPEO was not fully suppressed by P(LiMTFSI), and short-range repulsion between polymers was observed to dominate, leading to disordered concentration fluctuations. As more P(LiMTFSI) was introduced, electrostatic interactions were found to stabilize the blend morphology, enhance miscibility, and lead to a disordered phase with charge-correlated nanostructures, consistent with predictions from an SCFT-LS model previously proposed by Sing and coworkers. The temperature dependence of both the interdomain spacing and correlation length is also strongly influenced by blend composition r. Future work will investigate how the origin of the temperature effect influences the thermodynamics and nanostructure of SICPBs.

ASSOCIATED CONTENT

Supporting Information.

Synthetic route, NMR spectra, GPC trace, DSC, SANS, SAXS, fitting results (PDF)

AUTHOR INFORMATION

Corresponding Author

*Whitney Loo - Department of Chemical and Biological Engineering, University of Wisconsin—Madison, 1415 Engineering Drive, Madison, Wisconsin 53706, United States; Email: wloo@wisc.edu

Present Addresses

†Department of Chemical and Biological Engineering, University of Wisconsin—Madison, 1415 Engineering Drive, Madison, Wisconsin 53706, United States

Nomenclature

A, B	Scaling factors of correlation model
A', B'	Fitting parameters for temperature-dependent Flory-Huggins interaction parameter
B_i	Neutron scattering length density of species i
b_i	Neutron scattering length of species i
Đ	Dispersity
$I(q)$	Scattering intensity
k	adjustable parameter of Gordon-Taylor equation

k_B	Boltzmann's constant
l_i	Statistical segment length of species i (Å)
$M_{n,i}$	Molecular weight of species i
m	Lorentzian exponent
N_i	Degree of polymerization of species i
n	Porod exponent
$P_i(q)$	Form factor of species i
q	Scattering vector
q_0	Lorentzian peak position
$R_{g,i}$	Radius of gyration
r	Mixing ratio of P(LiMTFSI) to dPEO ($= [Li^+]/[dEO] = [P(LiMTFSI)]/[dPEO]$)
S_{ii}	Structure factor of species i
T	Absolute temperature (K)
T_g	Glass-transition temperature
T_m	Melting temperature
w_i	Weight fraction of species i

α_i	Chain stretching parameter
χ	Flory-Huggins interaction parameter
χ_{sc}	Flory-Huggins interaction parameter determined from SANS results
ξ	Correlation length of Lorentzian peak
λ	Wavelength of the x-ray/neutron
φ_i	Volume fraction of polymer i
ρ_i	Density of species i (g/cm^3)
θ	Scattering angle
v_i	Molar volume of species i
v_{ref}	Reference volume

ACKNOWLEDGMENT

This research was supported by the U.S. Department of Energy, Office of Basic Energy Sciences, Division of Materials Sciences and Engineering under Award #DE-SC0025449. The authors gratefully acknowledge the use of facilities and instrumentation at Wisconsin Centers for Nanoscale Technology (wcnt.wisc.edu) partially supported by the NSF through the University of Wisconsin Materials Research Science and Engineering Center (DMR-2309000). The Bruker AVANCE III 400 NMR spectrometer was supported by NSF grant CHE-1048642. We appreciate the assistance from Prof. AJ Boydston with the differential scanning calorimetry. This research

used resources at the High Flux Isotope Reactor, a DOE Office of Science User Facility operated by the Oak Ridge National Laboratory. The beam time was allocated to CG-2 (GP-SANS) on proposal number IPTS-32043-1.

REFERENCES

(1) Song, Z.; Chen, F.; Martinez-Ibañez, M.; Feng, W.; Forsyth, M.; Zhou, Z.; Armand, M.; Zhang, H. A Reflection on Polymer Electrolytes for Solid-State Lithium Metal Batteries. *Nat. Commun.* **2023**, *14* (1), 4884. https://doi.org/10.1038/s41467-023-40609-y.

(2) Bennington, P.; Deng, C.; Sharon, D.; Webb, M. A.; de Pablo, J. J.; Nealey, P. F.; Patel, S. N. Role of Solvation Site Segmental Dynamics on Ion Transport in Ethylene-Oxide Based Side-Chain Polymer Electrolytes. *J. Mater. Chem. A* **2021**, *9* (15), 9937–9951. https://doi.org/10.1039/D1TA00899D.

(3) Wright, P. V. Electrical Conductivity in Ionic Complexes of Poly(Ethylene Oxide). *Br. Polym. J.* **1975**, *7* (5), 319–327. https://doi.org/10.1002/pi.4980070505.

(4) Hallinan, D. T.; Balsara, N. P. Polymer Electrolytes. *Annu. Rev. Mater. Res.* **2013**, *43* (1), 503–525. https://doi.org/10.1146/annurev-matsci-071312-121705.

(5) Pesko, D. M.; Timachova, K.; Bhattacharya, R.; Smith, M. C.; Villaluenga, I.; Newman, J.; Balsara, N. P. Negative Transference Numbers in Poly(Ethylene Oxide)-Based Electrolytes. *J. Electrochem. Soc.* **2017**, *164* (11), E3569. https://doi.org/10.1149/2.0581711jes.

(6) Xie, T.; France-Lanord, A.; Wang, Y.; Lopez, J.; Stolberg, M. A.; Hill, M.; Leverick, G. M.; Gomez-Bombarelli, R.; Johnson, J. A.; Shao-Horn, Y.; Grossman, J. C. Accelerating Amorphous Polymer Electrolyte Screening by Learning to Reduce Errors in Molecular

Dynamics Simulated Properties. *Nat. Commun.* **2022**, *13* (1), 3415. https://doi.org/10.1038/s41467-022-30994-1.

(7) Gao, J.; Wang, C.; Han, D.-W.; Shin, D.-M. Single-Ion Conducting Polymer Electrolytes as a Key Jigsaw Piece for next-Generation Battery Applications. *Chem. Sci.* **2021**, *12* (40), 13248–13272. https://doi.org/10.1039/D1SC04023E.

(8) Stolz, L.; Hochstädt, S.; Röser, S.; Hansen, M. R.; Winter, M.; Kasnatscheew, J. Single-Ion versus Dual-Ion Conducting Electrolytes: The Relevance of Concentration Polarization in Solid-State Batteries. *ACS Appl. Mater. Interfaces* **2022**, *14* (9), 11559–11566. https://doi.org/10.1021/acsami.2c00084.

(9) Paren, B. A.; Nguyen, N.; Ballance, V.; Hallinan, D. T.; Kennemur, J. G.; Winey, K. I. Superionic Li-Ion Transport in a Single-Ion Conducting Polymer Blend Electrolyte. *Macromolecules* **2022**, *55* (11), 4692–4702. https://doi.org/10.1021/acs.macromol.2c00459.

(10) Yang, M.; Epps, T. H. I. Solid-State, Single-Ion Conducting, Polymer Blend Electrolytes with Enhanced Li+ Conduction, Electrochemical Stability, and Limiting Current Density. *Chem. Mater.* **2024**, *36* (4), 1855–1869. https://doi.org/10.1021/acs.chemmater.3c02389.

(11) Timachova, K.; Villaluenga, I.; Cirrincione, L.; Gobet, M.; Bhattacharya, R.; Jiang, X.; Newman, J.; Madsen, L. A.; Greenbaum, S. G.; Balsara, N. P. Anisotropic Ion Diffusion and Electrochemically Driven Transport in Nanostructured Block Copolymer Electrolytes. *J. Phys. Chem. B* **2018**, *122* (4), 1537–1544. https://doi.org/10.1021/acs.jpcb.7b11371.

(12) Sharon, D.; Deng, C.; Bennington, P.; Webb, M. A.; Patel, S. N.; de Pablo, J. J.; Nealey, P. F. Critical Percolation Threshold for Solvation-Site Connectivity in Polymer Electrolyte Mixtures. *Macromolecules* **2022**, *55* (16), 7212–7221. https://doi.org/10.1021/acs.macromol.2c00988.

(13) Loo, W. S.; Mongcopa, K. I.; Gribble, D. A.; Faraone, A. A.; Balsara, N. P. Investigating the Effect of Added Salt on the Chain Dimensions of Poly(Ethylene Oxide) through Small-Angle Neutron Scattering. *Macromolecules* **2019**, *52* (22), 8724–8732. https://doi.org/10.1021/acs.macromol.9b01509.

(14) Tucker, R. T.; Han, C. C.; Dobrynin, A. V.; Weiss, R. A. Small-Angle Neutron Scattering Analysis of Blends with Very Strong Intermolecular Interactions: Polyamide/Ionomer Blends. *Macromolecules* **2003**, *36* (12), 4404–4410. https://doi.org/10.1021/ma0341972.

(15) Kumar, S.; Pineri, M. Interpretation of small-angle x-ray and neutron scattering data for perfluorosulfonated ionomer membranes. *J. Polym. Sci. Part B Polym. Phys.* **1986**, *24* (8), 1767–1782. https://doi.org/10.1002/polb.1986.090240812.

(16) Horkay, F.; Hammouda, B. Small-Angle Neutron Scattering from Typical Synthetic and Biopolymer Solutions. *Colloid Polym. Sci.* **2008**, *286* (6), 611–620. https://doi.org/10.1007/s00396-008-1849-3.

(17) Gao, K. W.; Loo, W. S.; Snyder, R. L.; Abel, B. A.; Choo, Y.; Lee, A.; Teixeira, S. C. M.; Garetz, B. A.; Coates, G. W.; Balsara, N. P. Miscible Polyether/Poly(Ether–Acetal) Electrolyte Blends. *Macromolecules* **2020**, *53* (14), 5728–5739. https://doi.org/10.1021/acs.macromol.0c00747.

(18) Shah, N. J.; He, L.; Gao, K. W.; Balsara, N. P. Thermodynamics and Phase Behavior of Poly(Ethylene Oxide)/Poly(Methyl Methacrylate)/Salt Blend Electrolytes Studied by Small-Angle Neutron Scattering. *Macromolecules* **2023**, *56* (7), 2889–2898. https://doi.org/10.1021/acs.macromol.2c02533.

(19) Lee, J.; Abdo, E. E.; Pratt, C.; Kwon, Y. H.; Lim, J.; Patel, V.; He, L.; Balsara, N. P. Completely Miscible Polymer Blend Electrolyte Studied by Small-Angle Neutron Scattering.

Macromolecules **2024**, *57* (22), 10549–10556. https://doi.org/10.1021/acs.macromol.4c01714.

(20) Jia, D.; Muthukumar, M.; Cheng, H.; Han, C. C.; Hammouda, B. Concentration Fluctuations near Lower Critical Solution Temperature in Ternary Aqueous Solutions. *Macromolecules* **2017**, *50* (18), 7291–7298. https://doi.org/10.1021/acs.macromol.7b01502.

(21) Reichart, G. C.; Graessley, W. W.; Register, R. A.; Krishnamoorti, R.; Lohse, D. J. Measurement of Thermodynamic Interactions in Ternary Polymer Blends by Small-Angle Neutron Scattering. *Macromolecules* **1997**, *30* (11), 3363–3368. https://doi.org/10.1021/ma9616571.

(22) Sing, C. E.; Zwanikken, J. W.; de la Cruz, M. O. Theory of Melt Polyelectrolyte Blends and Block Copolymers: Phase Behavior, Surface Tension, and Microphase Periodicity. *J. Chem. Phys.* **2015**, *142* (3), 034902. https://doi.org/10.1063/1.4905830.

(23) Kong, X.; Qin, J. Microphase Separation in Neutral Homopolymer Blends Induced by Salt-Doping. *Macromolecules* **2023**, *56* (1), 254–262. https://doi.org/10.1021/acs.macromol.2c02198.

(24) Fang, Y. N.; Rumyantsev, A. M.; Neitzel, A. E.; Liang, H.; Heller, W. T.; Nealey, P. F.; Tirrell, M. V.; de Pablo, J. J. Scattering Evidence of Positional Charge Correlations in Polyelectrolyte Complexes. *Proc. Natl. Acad. Sci.* **2023**, *120* (32), e2302151120. https://doi.org/10.1073/pnas.2302151120.

(25) Grzetic, D. J.; Delaney, K. T.; Fredrickson, G. H. Electrostatic Manipulation of Phase Behavior in Immiscible Charged Polymer Blends. *Macromolecules* **2021**, *54* (6), 2604–2616. https://doi.org/10.1021/acs.macromol.1c00095.

(26) Rumyantsev, A. M.; Johner, A. Electrostatically Stabilized Microstructures: From Clusters to Necklaces to Bulk Microphases. *ACS Macro Lett.* **2025**, *14* (4), 472–483. https://doi.org/10.1021/acsmacrolett.4c00834.

(27) Rumyantsev, A. M.; Gavrilov, A. A.; Kramarenko, E. Yu. Electrostatically Stabilized Microphase Separation in Blends of Oppositely Charged Polyelectrolytes. *Macromolecules* **2019**, *52* (19), 7167–7174. https://doi.org/10.1021/acs.macromol.9b00883.

(28) Le, M. L.; Grzetic, D. J.; Delaney, K. T.; Yang, K.-C.; Xie, S.; Fredrickson, G. H.; Chabinyc, M. L.; Segalman, R. A. Electrostatic Interactions Control the Nanostructure of Conjugated Polyelectrolyte–Polymeric Ionic Liquid Blends. *Macromolecules* **2022**, *55* (18), 8321–8331. https://doi.org/10.1021/acs.macromol.2c01142.

(29) Sing, C. E.; Zwanikken, J. W.; Olvera de la Cruz, M. Ion Correlation-Induced Phase Separation in Polyelectrolyte Blends. *ACS Macro Lett.* **2013**, *2* (11), 1042–1046. https://doi.org/10.1021/mz400511r.

(30) Sing, C. E.; Olvera de la Cruz, M. Polyelectrolyte Blends and Nontrivial Behavior in Effective Flory–Huggins Parameters. *ACS Macro Lett.* **2014**, *3* (8), 698–702. https://doi.org/10.1021/mz500202n.

(31) Gennes, P. G. de. Theory of X-Ray Scattering by Liquid Macromolecules with Heavy Atom Labels. *J. Phys.* **1970**, *31* (2–3), 235–238. https://doi.org/10.1051/jphys:01970003102-3023500.

(32) Hammouda, B. PROBING NANOSCALE STRUCTURES – THE SANS TOOLBOX.

(33) Lee, O. A.; McBride, M. K.; Ticknor, M.; Sharpes, J.; Hayward, R. C. Pendent Sulfonylimide Ionic Liquid Monomers and Ionoelastomers via SuFEx Click Chemistry. *Chem. Mater.* **2023**, *35* (23), 10030–10040. https://doi.org/10.1021/acs.chemmater.3c02038.

(34) Heller, W. T.; Cuneo, M.; Debeer-Schmitt, L.; Do, C.; He, L.; Heroux, L.; Littrell, K.; Pingali, S. V.; Qian, S.; Stanley, C.; Urban, V. S.; Wu, B.; Bras, W. The Suite of Small-Angle Neutron Scattering Instruments at Oak Ridge National Laboratory. *J. Appl. Crystallogr.* **2018**, *51* (2), 242–248. https://doi.org/10.1107/S1600576718001231.

(35) Heller, W. T.; Hetrick, J.; Bilheux, J.; Calvo, J. M. B.; Chen, W.-R.; DeBeer-Schmitt, L.; Do, C.; Doucet, M.; Fitzsimmons, M. R.; Godoy, W. F.; Granroth, G. E.; Hahn, S.; He, L.; Islam, F.; Lin, J.; Littrell, K. C.; McDonnell, M.; McGaha, J.; Peterson, P. F.; Pingali, S. V.; Qian, S.; Savici, A. T.; Shang, Y.; Stanley, C. B.; Urban, V. S.; Whitfield, R. E.; Zhang, C.; Zhou, W.; Billings, J. J.; Cuneo, M. J.; Leal, R. M. F.; Wang, T.; Wu, B. Drtsans: The Data Reduction Toolkit for Small-Angle Neutron Scattering at Oak Ridge National Laboratory. *SoftwareX* **2022**, *19*. https://doi.org/10.1016/j.softx.2022.101101.

(36) *Physical Properties of Polymers Handbook*; Mark, J. E., Ed.; Springer: New York, NY, 2007. https://doi.org/10.1007/978-0-387-69002-5.

(37) Olmedo-Martínez, J. L.; Porcarelli, L.; Alegría, Á.; Mecerreyes, D.; Müller, A. J. High Lithium Conductivity of Miscible Poly(Ethylene Oxide)/Methacrylic Sulfonamide Anionic Polyelectrolyte Polymer Blends. *Macromolecules* **2020**, *53* (11), 4442–4453. https://doi.org/10.1021/acs.macromol.0c00703.

(38) Arrighi, V.; Cowie, J. M. G.; Fuhrmann, S.; Youssef, A. Miscibility Criterion in Polymer Blends and Its Determination. In *Encyclopedia of Polymer Blends*; John Wiley & Sons, Ltd, 2010; pp 153–198. https://doi.org/10.1002/9783527805204.ch5.

(39) Mukri, N. I.; Velayutham, T. S.; Gan, W. C.; Abd Majid, W. H. Miscibility and Crystallinity Study of Poly(Vinylidene Fluoride) / Poly(L-Lactic Acid) Polymer Blend. *Mater. Today Proc.* **2018**, *5*, S130–S136. https://doi.org/10.1016/j.matpr.2018.08.054.

(40) Platen, K.; Langer, F.; Bayer, R.; Hollmann, R.; Schwenzel, J.; Busse, M. Influence of Molecular Weight and Lithium Bis(Trifluoromethanesulfonyl)Imide on the Thermal Processability of Poly(Ethylene Oxide) for Solid-State Electrolytes. *Polymers* **2023**, *15* (16), 3375. https://doi.org/10.3390/polym15163375.

(41) Zheng, Q.; Pesko, D. M.; Savoie, B. M.; Timachova, K.; Hasan, A. L.; Smith, M. C.; Miller, T. F. I.; Coates, G. W.; Balsara, N. P. Optimizing Ion Transport in Polyether-Based Electrolytes for Lithium Batteries. *Macromolecules* **2018**, *51* (8), 2847–2858. https://doi.org/10.1021/acs.macromol.7b02706.

(42) Ollier, R.; Stocchi, A.; Rodriguez, E.; Alvarez, V. Effect of Thermoplastic Incorporation on the Performance of Thermosetting Matrix. *Mater. Sci. Appl.* **2012**, *3* (7), 442–447. https://doi.org/10.4236/msa.2012.37062.

(43) Choi, U. H.; Liang, S.; O'Reilly, M. V.; Winey, K. I.; Runt, J.; Colby, R. H. Influence of Solvating Plasticizer on Ion Conduction of Polysiloxane Single-Ion Conductors. *Macromolecules* **2014**, *47* (9), 3145–3153. https://doi.org/10.1021/ma500146v.

(44) Nguyen, N.; Blatt, M. P.; Kim, K.; Hallinan, D. T.; Kennemur, J. G. Investigating Miscibility and Lithium Ion Transport in Blends of Poly(Ethylene Oxide) with a Polyanion Containing Precisely-Spaced Delocalized Charges. *Polym. Chem.* **2022**, *13* (29), 4309–4323. https://doi.org/10.1039/D2PY00605G.

(45) Thelen, J. L.; Inceoglu, S.; Venkatesan, N. R.; Mackay, N. G.; Balsara, N. P. Relationship between Ion Dissociation, Melt Morphology, and Electrochemical Performance of Lithium and Magnesium Single-Ion Conducting Block Copolymers. *Macromolecules* **2016**, *49* (23), 9139–9147. https://doi.org/10.1021/acs.macromol.6b01886.

(46) Balsara, N. P.; Lohse, D. J.; Graessley, W. W.; Krishnamoorti, R. Small-angle Neutron Scattering by Partially Deuterated Polymers and Their Blends. *J. Chem. Phys.* **1994**, *100* (5), 3905–3910. https://doi.org/10.1063/1.466325.

(47) Xie, S.; Zhang, B.; Mao, Y.; He, L.; Hong, K.; Bates, F. S.; Lodge, T. P. Influence of Added Salt on Chain Conformations in Poly(Ethylene Oxide) Melts: SANS Analysis with Complications. *Macromolecules* **2020**, *53* (16), 7141–7149. https://doi.org/10.1021/acs.macromol.0c01194.

(48) Lee, J.; Gao, K. W.; Shah, N. J.; Kang, C.; Snyder, R. L.; Abel, B. A.; He, L.; Teixeira, S. C. M.; Coates, G. W.; Balsara, N. P. Relationship between Ion Transport and Phase Behavior in Acetal-Based Polymer Blend Electrolytes Studied by Electrochemical Characterization and Neutron Scattering. *Macromolecules* **2022**, *55* (24), 11023–11033. https://doi.org/10.1021/acs.macromol.2c01724.

(49) Rojas, A. A.; Inceoglu, S.; Mackay, N. G.; Thelen, J. L.; Devaux, D.; Stone, G. M.; Balsara, N. P. Effect of Lithium-Ion Concentration on Morphology and Ion Transport in Single-Ion-Conducting Block Copolymer Electrolytes. *Macromolecules* **2015**, *48* (18), 6589–6595. https://doi.org/10.1021/acs.macromol.5b01193.

(50) Inceoglu, S.; Rojas, A. A.; Devaux, D.; Chen, X. C.; Stone, G. M.; Balsara, N. P. Morphology–Conductivity Relationship of Single-Ion-Conducting Block Copolymer Electrolytes for Lithium Batteries. *ACS Macro Lett.* **2014**, *3* (6), 510–514. https://doi.org/10.1021/mz5001948.

(51) Akcasu, A. Z.; Tombakoglu, M. Dynamics of Copolymer and Homopolymer Mixtures in Bulk and in Solution via the Random Phase Approximation. *Macromolecules* **1990**, *23* (2), 607–612. https://doi.org/10.1021/ma00204a038.

(52) Hammouda, B. Random Phase Approximation for Compressible Polymer Blends. *Proc. Second Internatinal Discuss. Meet. Relax. Complex Syst.* **1994**, *172–174*, 927–931. https://doi.org/10.1016/0022-3093(94)90600-9.

(53) Krevelen, D. W. van; Nijenhuis, K. te. *Properties of Polymers: Their Correlation with Chemical Structure: Their Numerical Estimation and Prediction from Additive Group Contributions*, 4th, completely rev. ed.; Elsevier: Amsterdam, 2009.

(54) Wang, D.; Lal, J.; Moses, D.; Bazan, G. C.; Heeger, A. J. Small Angle Neutron Scattering (SANS) Studies of a Conjugated Polyelectrolyte in Aqueous Solution. *Chem. Phys. Lett.* **2001**, *348* (5), 411–415. https://doi.org/10.1016/S0009-2614(01)01151-4.

(55) Hammouda, B.; Horkay, F.; Becker, M. L. Clustering and Solvation in Poly(Acrylic Acid) Polyelectrolyte Solutions. *Macromolecules* **2005**, *38* (5), 2019–2021. https://doi.org/10.1021/ma047960g.

(56) Hammouda, B.; Ho, D.; Kline, S. SANS from Poly(Ethylene Oxide)/Water Systems. *Macromolecules* **2002**, *35* (22), 8578–8585. https://doi.org/10.1021/ma011657n.

(57) Knychała, P.; Timachova, K.; Banaszak, M.; Balsara, N. P. 50th Anniversary Perspective: Phase Behavior of Polymer Solutions and Blends. *Macromolecules* **2017**, *50* (8), 3051–3065. https://doi.org/10.1021/acs.macromol.6b02619.

(58) Markarian, M. Z.; Hariri, H. H.; Reisch, A.; Urban, V. S.; Schlenoff, J. B. A Small-Angle Neutron Scattering Study of the Equilibrium Conformation of Polyelectrolytes in Stoichiometric Saloplastic Polyelectrolyte Complexes. *Macromolecules* **2012**, *45* (2), 1016–1024. https://doi.org/10.1021/ma2022666.

(59) Kosgallana, C.; Senanayake, M.; Mohottalalage, S. S.; Wijesinghe, S.; He, L.; Grest, G. S.; Perahia, D. Clustering Effects on the Structure of Ionomer Solutions: A Combined SANS and

Simulations Study. *Macromolecules* **2024**, *57* (4), 1688–1698. https://doi.org/10.1021/acs.macromol.3c01646.

(60) Wang, W.; Tudryn, G. J.; Colby, R. H.; Winey, K. I. Thermally Driven Ionic Aggregation in Poly(Ethylene Oxide)-Based Sulfonate Ionomers. *J. Am. Chem. Soc.* **2011**, *133* (28), 10826–10831. https://doi.org/10.1021/ja201405v.

(61) Ylitalo, A. S.; Balzer, C.; Zhang, P.; Wang, Z.-G. Electrostatic Correlations and Temperature-Dependent Dielectric Constant Can Model LCST in Polyelectrolyte Complex Coacervation. *Macromolecules* **2021**, *54* (24), 11326–11337. https://doi.org/10.1021/acs.macromol.1c02000.